PROCEEDINGS B

rspb.royalsocietypublishing.org

Research

Cite this article: Padmanabhan P, Goodhill GJ. 2018 Axon growth regulation by a bistable molecular switch. *Proc. R. Soc. B* **285**: 20172618.
http://dx.doi.org/10.1098/rspb.2017.2618

Received: 23 November 2017
Accepted: 19 March 2018

Subject Category:
Neuroscience and cognition

Subject Areas:
neuroscience, theoretical biology

Keywords:
axon guidance, growth cone, signal-transduction, bistability, stochastic switches

Author for correspondence:
Geoffrey J. Goodhill
e-mail: g.goodhill@uq.edu.au

Electronic supplementary material is available online at https://dx.doi.org/10.6084/m9.figshare.c.4041485.

THE ROYAL SOCIETY PUBLISHING

Axon growth regulation by a bistable molecular switch

Pranesh Padmanabhan[1] and Geoffrey J. Goodhill[1,2]

[1]Queensland Brain Institute, and [2]School of Mathematics and Physics, The University of Queensland, St Lucia, Brisbane, Queensland 4072, Australia

PP, 0000-0001-5569-8731; GJG, 0000-0001-9789-9355

For the brain to function properly, its neurons must make the right connections during neural development. A key aspect of this process is the tight regulation of axon growth as axons navigate towards their targets. Neuronal growth cones at the tips of developing axons switch between growth and paused states during axonal pathfinding, and this switching behaviour determines the heterogeneous axon growth rates observed during brain development. The mechanisms controlling this switching behaviour, however, remain largely unknown. Here, using mathematical modelling, we predict that the molecular interaction network involved in axon growth can exhibit bistability, with one state representing a fast-growing growth cone state and the other a paused growth cone state. Owing to stochastic effects, even in an unchanging environment, model growth cones reversibly switch between growth and paused states. Our model further predicts that environmental signals could regulate axon growth rate by controlling the rates of switching between the two states. Our study presents a new conceptual understanding of growth cone switching behaviour, and suggests that axon guidance may be controlled by both cell-extrinsic factors and cell-intrinsic growth regulatory mechanisms.

1. Introduction

Brain function depends critically on the precise patterns of neural wiring during development, and wiring defects lead to several neurological disorders [1]. The tight regulation of axon growth is crucial for correct brain wiring [2–4]. Although a large number of molecules involved in axon growth have been identified [5,6], a systems-level understanding of how these molecules interact to regulate axon growth is still lacking.

Growth cones at the tips of developing axons sense environmental signals and regulate directed axon growth [7]. During axonal pathfinding *in vivo*, growth cones often switch between rapid growth and paused states [8–11]. Importantly, the time spent by growth cones in the two states appears to primarily determine the heterogeneous axon growth rates observed at different locations in the developing brain [8–11]. This growth cone switching behaviour thus appears to control axon growth rate *in vivo*. The mechanisms underlying this switching behaviour, however, remain largely unknown.

One possibility is that it is simply due to changes in the environmental signals or physical interactions between growth cones and their environment. However, growth cones spontaneously switch between growth and paused states even in the nearly constant environmental condition of cell cultures [12–14]. Thus, in addition to axon growth regulation by environmental factors, there also appears to be a contribution from cell-intrinsic mechanisms.

A critical control point that couples intracellular signalling to cytoskeleton dynamics and growth cone motility is the integrin-mediated point contact (PC) adhesions formed between the growth cone and extracellular matrix (ECM). In particular, PCs couple the actin cytoskeletal network with the ECM, reduce the retrograde flow of F-actin and generate traction force required for axon growth [15]. Furthermore, axon growth rate is strongly correlated with PC adhesion dynamics [16]. Several axon guidance cues, including soluble and substrate-bound cues, alter

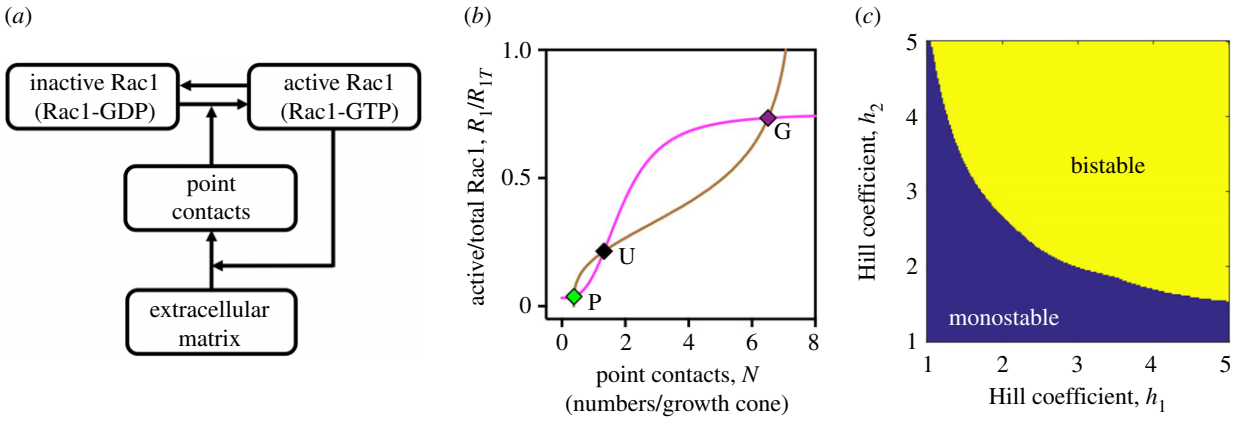

Figure 1. Bistability in the point contact adhesion dynamics. (*a*) Schematic of the model. The rho GTPase Rac1 shuttles between a GTP-bound active state and a GDP-bound inactive state. Active Rac1 promotes PC assembly, whereas PCs recruit PIX via PXN to activate Rac1. (*b*) Model predictions of concentration-effect curves showing the steady-state levels of active Rac1 for different fixed values of PCs (magenta line) and the steady-state number of PCs for different fixed levels of active Rac1 (brown line). The points of intersection mark the steady states of the model. G (purple diamond) and P (green diamond) are the growth and paused stable steady states of the model growth cone, respectively, and U (black diamond) is an unstable steady state. (*c*) 2D bifurcation phase diagram for the model, with Hill coefficients along the *x*-axis and the *y*-axis. The model is monostable in the blue and bistable in the yellow region. In (*b*), $h_1 = h_2 = 3$. The other model parameter values are provided in the electronic supplementary material, table S1. (Online version in colour.)

axon growth rate by directly regulating PC adhesion dynamics, and integrin-mediated adhesion to the ECM is important for axonal pathfinding *in vivo* [17].

PCs are composed of a number of signalling and scaffolding proteins. A key component of PCs involved in axon growth and guidance is paxillin (PXN). PXN recruits the guanine nucleotide exchanging factor PIX via paxillin kinase linker (PKL or GIT2), and the PXN-GIT-PIX complex activates the rho GTPase Rac1 in growth cones [18]. Active Rac1 promotes the assembly of growth cone PCs [19] and induces phosphorylation of p21-activated kinase (PAK) [20]. Phosphorylation of PXN by phosphorylated PAK enhances PXN-mediated PIX recruitment [21]. Thus, these molecular interactions involved in PC adhesion dynamics consist of positive feedback loops. Such loops are ubiquitously found in biological systems and regulate several cellular processes, including cell-cycle transitions [22], cell migration [23], cellular phenotypic switching [24], synaptic plasticity [25] and neuronal symmetry breaking [26]. In particular, positive feedback loops in the Rac1 and PAK circuit have been suggested to regulate adhesion and membrane protrusion dynamics at the front end of migrating cells [21,27,28]. However, the functional consequences of positive feedback loops in regulating axon growth remain to be investigated.

Here, we developed a simplified mathematical model of PC adhesion dynamics and predict that the positive feedback loop in PC adhesion dynamics could lead to bistable growth and paused states of the growth cone. We then show that, due to stochastic effects, the model growth cones spontaneously switch between the two states. Our model predicts that environmental signals could regulate axon growth by altering the bistable property of the intracellular signalling network and the time spent in the growth and paused states. Thus, axon guidance may depend critically on a balance between intrinsic bistability and environmental signals.

2. Mathematical model of growth cone point contact adhesion dynamics

We constructed a simplified mathematical model to describe growth cone point contact (PC) adhesion dynamics (figure 1*a*). Our model consists of two variables, describing the level of active Rac1 (R_1) and the number of PCs (N) within a growth cone. Active Rac1 promotes the assembly of PCs [19], but the molecular steps involved in this process are not known. PCs, on the other hand, recruit PXN, which in turn recruit PIX. Recruited PIX acts as a Guanazine Exchange Factor (GEF) to activate Rac1 [18]. We modelled Rac1-mediated PC assembly and PC-dependent Rac1 activation using Hill functions, which are commonly used in modelling intracellular signalling networks, especially when details of molecular steps are not known [29,30]. The time evolution of N and R_1 is given by

$$\frac{dN}{dt} = a\left(x + (1-x)\frac{(R_1)^{h_1}}{(K_{R1})^{h_1} + (R_1)^{h_1}}\right) - dN \tag{2.1}$$

and

$$\frac{dR_1}{dt} = b_0(R_{1T} - R_1) + k_{ar}\frac{(N)^{h_2}}{(K_N)^{h_2} + (N)^{h_2}} \times (R_{1T} - R_1) - k_{dr}R_1. \tag{2.2}$$

Here, a is the point contact assembly rate constant, and x, which can vary between 0 and 1, determines the dependence of PC assembly on the levels of active Rac1. When $x = 0$, the point contact assembly rate is fully dependent on the levels of active Rac1, and when $x = 1$, the point contact assembly rate is independent of levels of active Rac1. The strength of the feedback loops in the model is characterized by activation coefficients K_N and K_{R1}. Increasing the values of these parameters decreased the feedback loop strength and vice versa. d is the intrinsic PC disassembly rate constant, h_1 and h_2 are the Hill coefficients, b_0 is the basal Rac1 activation rate constant, R_{1T} is the total number of Rac1 in a growth cone, i.e. the sum of active and inactive Rac1, k_{ar} is the PC-dependent Rac1 activation constant, and k_{dr} is the Rac1 deactivation rate constant. For details on parameter estimation and model calculations see electronic supplementary material, supplementary materials and methods.

3. Results

(a) Point contact adhesion dynamics in the growth cone can exhibit bistability

The molecular interactions involved in PC adhesion dynamics consist of positive feedback loops. We developed a simple mathematical model to investigate the functional consequences of these loops (figure 1*a*). Our model consists of two coupled ordinary differential equations describing the levels of active Rac1 (Rac1-GTP), R_1, and the number of PCs, N, within a growth cone. Using model parameter values constrained, wherever possible, by experimental measurements (see electronic supplementary material, supplementary materials and methods and table S1), we investigated the steady-state properties of the model (equations (2.1) and (2.2)).

When there is ultrasensitivity in the positive feedback loop, i.e. for large values of Hill coefficients, the deterministic model could admit two stable steady states G (growth) and P (paused) and an unstable steady-state U. The level of active Rac1 and the number of point contacts are high in the stable steady-state G, intermediate in the unstable steady-state U, and low in the stable steady-state P (figure 1*b*). Active Rac1 is known to promote axon growth [19,31,32], whereas PCs promote axon growth by engaging the actin cytoskeletal network with the ECM [16,33]. We therefore associated the stable steady-state G to a fast advancing growth cone, and the stable steady-state P to a paused growth cone in our model. When there is no or weak ultrasensitivity in the positive feedback loop, i.e. for small values of Hill coefficients, the deterministic model admits only one stable steady state (figure 1*c*). How the model growth cone behaviour evolves with time depends on whether the model admits monostability or bistability, which we examined next.

(b) Growth cones stochastically switch between growth and paused states

Given the low number of point contacts per growth cone (less than 10 PCs per growth cone [18,19,34]), stochastic effects are likely to influence the temporal dynamics of the system [35,36]. We therefore performed stochastic simulations using the Gillespie algorithm (see electronic supplementary material, supplementary materials and methods), which has been extensively used to investigate the dynamics of cellular processes [27,37–41].

(i) Temporal dynamics of bistable growth cones

We first predicted the time evolution of the number of point contacts and the levels of active Rac1 within a growth cone when there is ultrasensitivity in the feedback loop (Hill coefficients, $h_1 = h_2 = 3$). We found that the model growth cone reversibly switched between the growth and paused steady states (figure 2*a*). The steady-state distribution estimated from a 10^6 min simulated trace had peaks centred on the deterministic stable steady-state values (figure 2*b*,*c*). We computed the expected time to switch from one stable steady state to another, i.e. the mean first passage time (MFPT), from 2000 simulated switches. The mean time spent by the model growth cone was $\tau_G = 83.8$ min in the growth state and $\tau_P = 45.3$ min in the paused state for the parameter values in the electronic supplementary material, table S1 (figure 2*d*).

The MFPTs in bistable systems are dependent on the number of components involved in the switching behaviour [39]. While the number of PCs per growth cone is constrained by experimental measurements [18,19,34], there is no direct measurement of the total number of Rac1 molecules per growth cone, R_{1T}. We therefore investigated the effect of R_{1T} on the switching behaviour. We scaled the Rac1-dependent activation coefficient K_{R1} with R_{1T}, such that increasing R_{1T} did not change the strength of the positive feedback loop and the steady-state number of PCs (electronic supplementary material, figure S1) and computed the MFPTs for different values of R_{1T}. We found that the MFPTs were not sensitive to changes in R_{1T} when the feedback strength was held constant (figure 2*d*), indicating that low number of PCs can lead to switching between the two stable states in our model.

(ii) Temporal dynamics of monostable growth cones

We next predicted the temporal dynamics of the model growth cone without ultrasensitivity in the feedback loop ($h_1 = h_2 = 1$). Recall that the deterministic model without ultrasensitivity admits only one stable steady state (figure 1*c*). When the PC assembly rates are high, the model growth cones did not show any switching behaviour (figure 3*a*). The steady-state distribution was unimodal, with the peak centred on the deterministic stable steady-state value (figure 3*b*,*c*). When the PC assembly rates are low, we found that the model growth cones displayed switching behaviour (figure 3*d*) and that the steady-state distribution had multiple peaks (figure 3*e*,*f*), even though the deterministic model is monostable.

This switching behaviour even in the absence of deterministic bistability is due to stochastic bistability [36,38], which can be understood as follows. The Rac1 GTPases activation/inactivation cycle happens at the timescale of seconds [29], whereas the PC assembly/disassembly dynamics occur at the timescale of minutes [19]. Because of this timescale separation, the levels of active Rac1, R_1, rapidly equilibrate to the discrete low number of PCs, N, present at any moment. When N stochastically becomes zero, the PC-dependent Rac1 activation rate becomes zero, leading to decreased levels of R_1 corresponding to the basal Rac1 activation rate. Consequently, the PC assembly rate is drastically reduced and the system is trapped in a state with $N = 0$ for a long duration. This kinetic trapping of the system at $N = 0$ leads to a peak at $N = 0$ and a peak at the basal levels of active Rac1 in the steady-state distributions (figure 3*e*,*f*). The other peaks in the steady-state distribution of R_1 correspond to discrete non-zero values of N. At large PC assembly rates, the stochastic fluctuations driving the system to $N = 0$ become rare, the switching behaviour disappears and the steady-state distributions become unimodal (figure 3*a*–*c*).

(iii) Temporal dynamics of a population of growth cones

Intrinsic variations, for example, in protein expression levels, lead to variations in model parameter values across growth cones. These variations could give rise to diverse growth cone behaviour even in a constant environmental condition. To predict the population-level behaviour, we simulated the temporal dynamics of a population of 1000 growth cones, each with a different set of model parameters. The parameter values were varied up to $\pm 25\%$ from the baseline values (electronic supplementary material, table S1) to generate different parameter sets. In these simulations, about 90% of growth

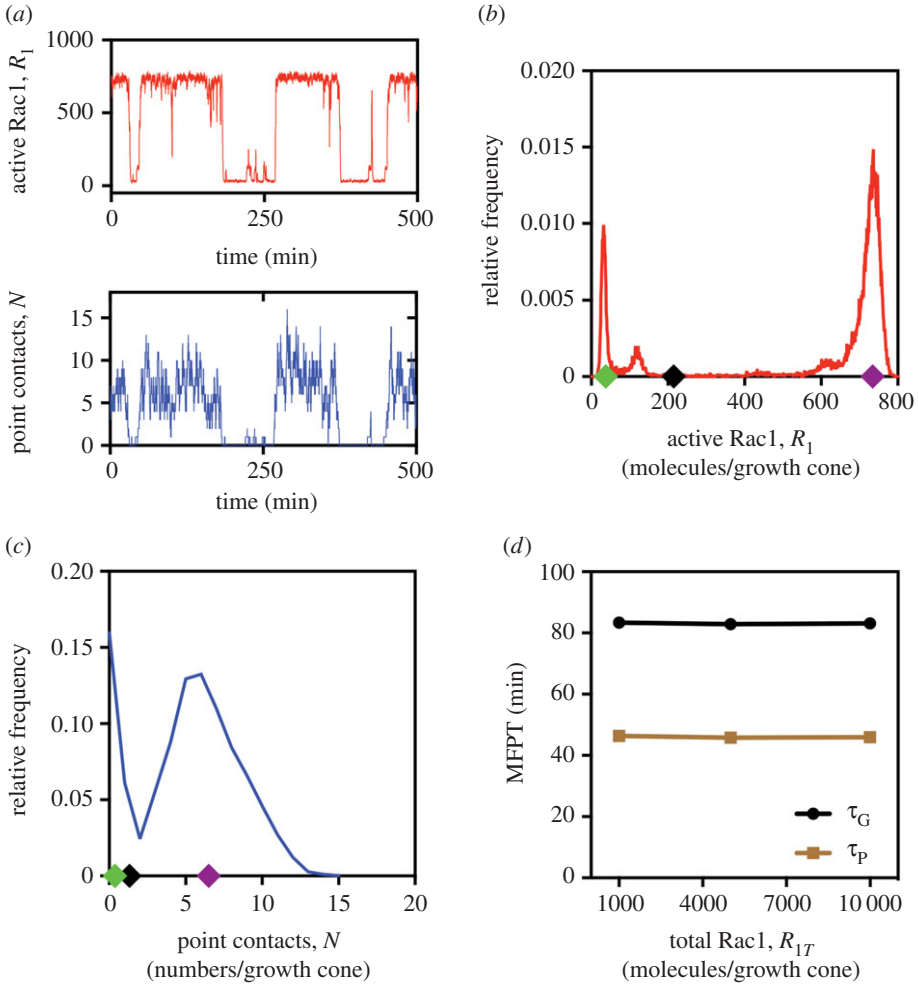

Figure 2. Temporal dynamics and steady-state distributions of a bistable growth cone. (*a*) An example of one simulation of the time evolution of the activated levels of Rac1 (top panel) and the number of point contact adhesions per growth cone (bottom panel). Steady-state distributions of (*b*) active Rac1 and (*c*) point contacts estimated from a 10^6 min simulated trace. The stable (green and magenta diamonds) and unstable (black diamond) steady-state values of the deterministic model are marked on the *x*-axis. (*d*) The MFPTs as a function of total Rac1 per growth cone, R_{1T}, with activation coefficient $K_{R1} = 0.4\ R_{1T}$. In (*a*–*d*), $h_1 = h_2 = 3$. τ_G and τ_P are the MFPTs for the growth and paused states, respectively. The other model parameter values are the same as in the electronic supplementary material, table S1. (Online version in colour.)

cones exhibited bistability and these could switch between the growth and paused states, albeit with different switching rates due to differences in parameter values across growth cones. The rest of the growth cones were monostable but could display switching behaviour due to stochastic bistability. Although individual growth cones stochastically switched between distinct states and behave differently (figure 4*a*), the number of PCs and the levels of active Rac1 averaged across growth cones remained nearly constant with time (figure 4*b*).

Thus, in our model, individual growth cones stochastically switch between distinct states even in a constant environmental condition. This switching behaviour is consistent with cell culture experiments where the growth cones alternate between growth and paused states in a nearly constant environmental condition, with the time spent in the growth and paused states ranging from tens of minutes to hours [12–14,42] (electronic supplementary material, table S2). Another key consequence of this switching behaviour is that, at any moment, both the growth and paused states of growth cones coexist at the population level even in constant environmental conditions. This is consistent with previous experimental observations that cell cultures consist of a mixed population of growth cones in the growth and paused states [13,42]. These results suggest that stochastic switching between distinct states of the intracellular signalling network could underlie the experimentally observed growth cone switching behaviour.

(c) Extracellular signals could regulate axon growth by controlling the growth cone state switching rates

Extracellular signals regulate axon growth by altering PC adhesion dynamics [19,34,43]. For instance, soluble brain-derived neurotrophic factor (BDNF) induces rapid clustering of β1-integrin receptors, facilitates PC formation and promotes axon growth, whereas soluble myelin-associated glycoprotein (MAG) prevents integrin receptor clustering and PC formation and inhibits axon growth [34]. In the model, the expression and clustering of integrin receptors are lumped into the PC adhesion assembly rate constant, a, and hence extracellular signals alter PC assembly rate. This is consistent with experimental observations that BDNF increases the PC adhesion assembly rate [44], whereas Sema3A, which inhibits axon growth, decreases the PC adhesion assembly rate [19]. Here, we considered a simple scenario where extracellular signals altered a alone in our model. In reality, growth cones receive combinations of growth-promoting and -inhibiting signals

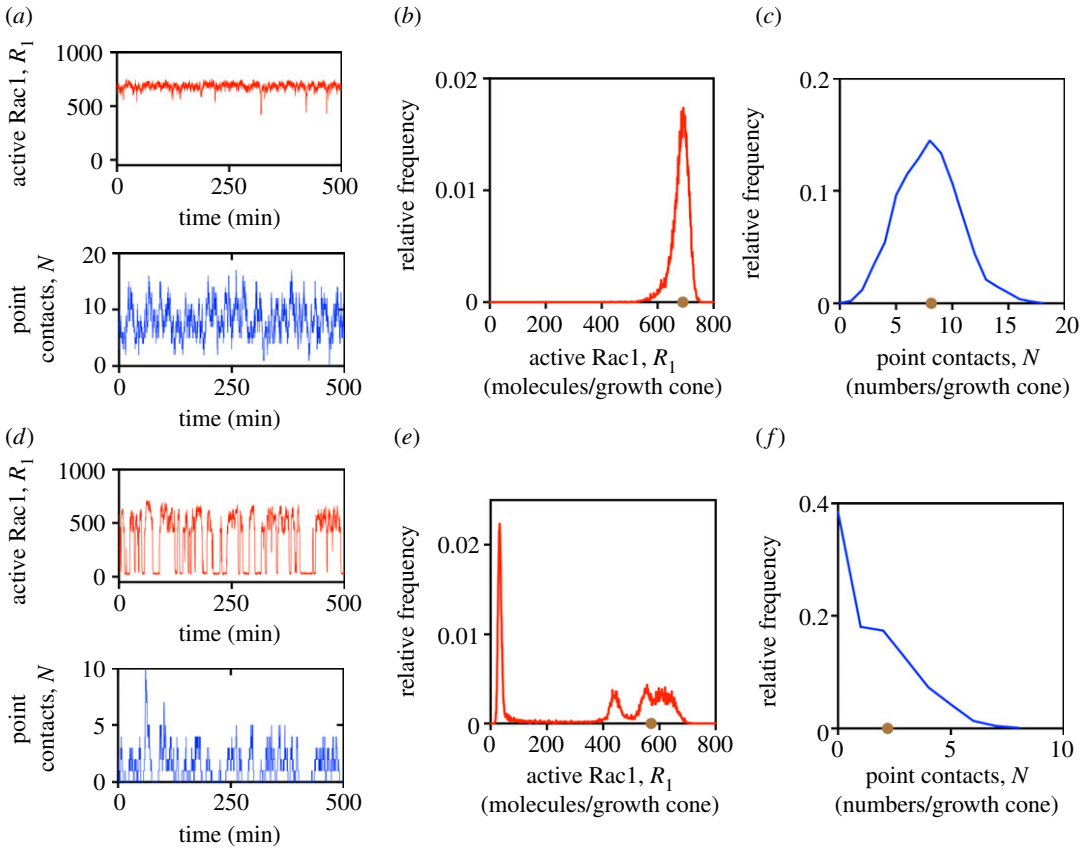

Figure 3. Temporal dynamics and steady-state distributions of a monostable growth cone. (*a*) An example of one simulation of the time evolution of the activated levels of Rac1, R_1, and the number of point contact adhesions per growth cone, N, with PC assembly rate constant $a = 5\ \text{min}^{-1}$. Steady-state distributions of (*b*) active Rac1 and (*c*) point contacts estimated from a 10^6 min simulated trace with $a = 5\ \text{min}^{-1}$. (*d*) An example of one simulation of the time evolution of the activated levels of Rac1 and the number of point contact adhesions per growth cone with $a = 1.5\ \text{min}^{-1}$. Steady-state distributions of (*e*) active Rac1 and (*f*) point contacts estimated from a 10^6 min simulated trace with $a = 1.5\ \text{min}^{-1}$. In (*b*,*c*,*e*,*f*), the stable steady-state value (brown circle) of the deterministic model is marked on the *x*-axis. In (*a*–*f*), $h_1 = h_2 = 1$. The other model parameter values are the same as in the electronic supplementary material, table S1. (Online version in colour.)

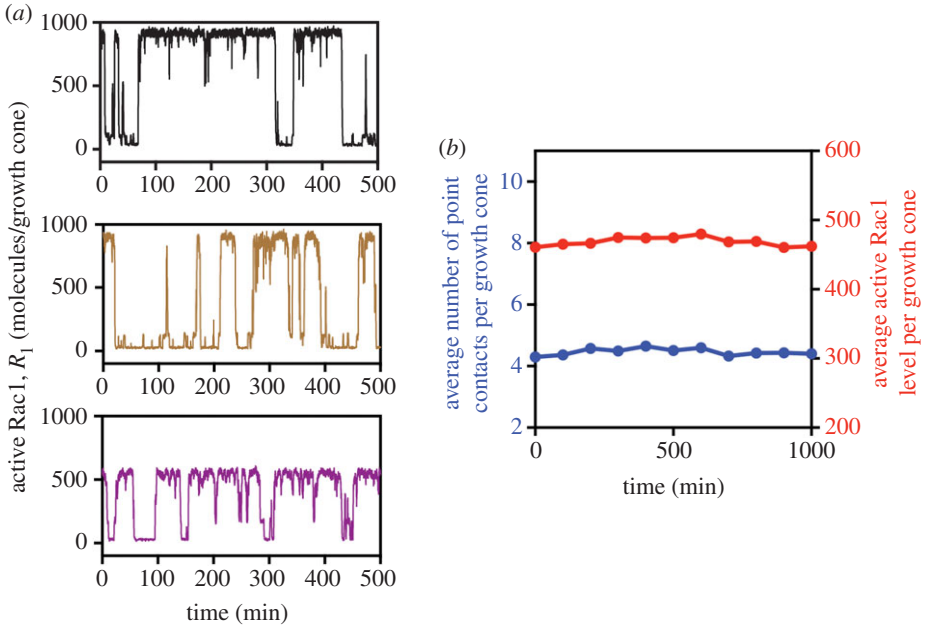

Figure 4. Temporal dynamics of a population of growth cones. (*a*) Three examples of simulation of the time evolution of the activated levels of Rac1, R_1. (*b*) The number of point contacts and the levels of active Rac1 averaged across 1000 growth cones. The parameter set for each growth cone was generated by randomly varying parameter values up to $\pm 25\%$ from the baseline values provided in the electronic supplementary material, table S1. (Online version in colour.)

from the environment [45], but here we focus on how growth cones execute growth decisions in response to one integrated signal that alters *a*.

We first examined the effect of extracellular signals on the steady-state properties of the model with ultrasensitivity in the feedback loop. For low values of *a*, the deterministic

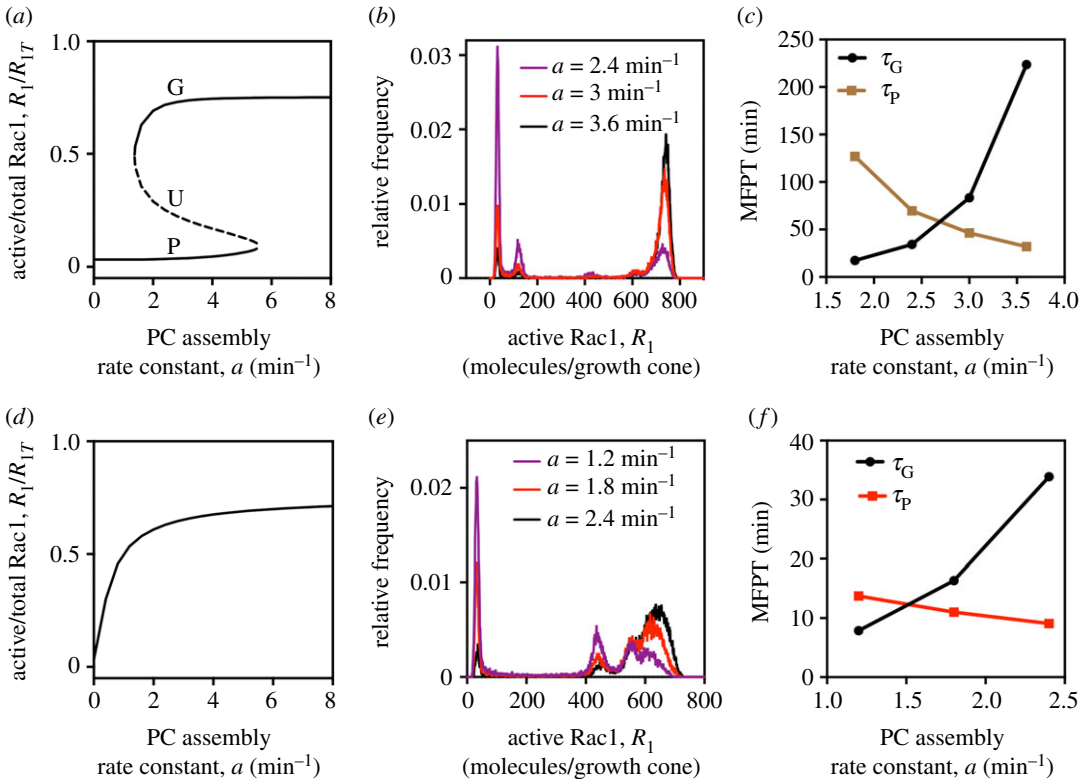

Figure 5. Influence of extracellular signals on the growth cone switching behaviour. (*a*) Deterministic steady-state levels of active Rac1, R_1, for different values of PC assembly rate constant, a, with $h_1 = h_2 = 3$. G is the growth stable steady state, P is the paused stable steady state and U is the unstable steady state. (*b*) Steady-state distributions of active Rac1 for different values of a with $h_1 = h_2 = 3$. (*c*) The MFPTs for different values of a with $h_1 = h_2 = 3$. (*d*) Deterministic steady-state levels of active Rac1 for different values of a with $h_1 = h_2 = 1$. (*e*) Steady-state distributions of active Rac1 for different values of a with $h_1 = h_2 = 1$. (*f*) The MFPTs for different values of a with $h_1 = h_2 = 1$. τ_G and τ_P are the MFPTs for the growth and paused states, respectively. Model parameter values other than a, h_1 and h_2 are the same as in the electronic supplementary material, table S1. (Online version in colour.)

model admitted only the paused steady state (figure 5*a* and electronic supplementary material, figure S2*a*). In this case, the extracellular signal strength is not sufficient to trigger the positive feedback loop. For high values of a, the deterministic model admitted only the growth steady state. In this case, the signal strength is strong enough to keep the positive feedback loop always activated (figure 5*a* and electronic supplementary material, figure S2*a*). For intermediate values of a, the deterministic model exhibited bistability. We found in our stochastic simulations that varying the extracellular signal strength altered the growth cone switching behaviour (figure 5*b*,*c* and electronic supplementary material, figure S2*b*). Increasing growth-promoting signal strength by increasing a biased the steady-state distribution towards the growth state, increased the time spent by the model growth cone in the growth state and decreased the time spent in the paused state. Conversely, increasing growth inhibitory signal strength by decreasing a biased the steady-state distribution towards the paused state, decreased the time spent by the model growth cone in the growth state and increased the time spent in the paused state.

We next considered the influence of extracellular signals on the steady-state properties of the model without ultrasensitivity (figure 5*d*,*e* and electronic supplementary material, figure S2*c*,*d*). For all values of a, the deterministic model admitted only one stable state, and the steady-state value increased with a. For low values of a, the model growth cone displayed stochastic switching behaviour. Varying the extracellular signal strength by varying a altered the time spent by the model growth cone in distinct states (figure 5*d*,*e* and electronic supplementary material, figure S2*c*,*d*). At the population level, the average number of PCs and level of active Rac1 per growth cone increased with a (electronic supplementary material, figure S2*e*–*g*).

Extracellular signals could potentially also alter other model parameter values. For instance, netrin-1 binding to its receptor leads to the recruitment of the guanine exchange factor Trio and the activation of Rac1 [32]. Variations in other model parameters yielded changes in the steady-state distributions and the MFPTs similar to variations in a (electronic supplementary material, figure S3). Thus, in our model, external signals could alter individual or combinations of model parameters to bias the basin of attraction of steady states, alter the growth cone state switching rates and regulate axon growth.

4. Discussion

During brain development, growth cones at the distal ends of developing axons sense molecular cues in the environment and guide axons to their appropriate targets. Previous studies have observed that growth cones switch between growth and paused states *in vitro* [12–14,42] and during axonal pathfinding *in vivo* [8,9,46–48]. In the present study, we used mathematical modelling to present a new conceptual understanding of growth cone switching behaviour. Our study suggests that the growth cone switching behaviour is a consequence of a bistable switch in the intracellular network of molecular interactions and that cell-intrinsic, systems-level

mechanisms could be involved in axon growth regulation during brain development.

The bistable behaviour of the model is due to a network motif with a positive feedback loop between Rac1 activation and PC adhesion dynamics. Owing to limited quantitative knowledge of the multiple intermediate molecular steps involved in Rac1-mediated PC assembly and PC-dependent Rac1 activation, we have lumped all these intermediate steps into Hill functions. Once more quantitative information becomes available this approximation could be relaxed and the influence of these intermediate steps on growth cone switching behaviour could be determined. We note that growth inhibitory guidance cues could also regulate axon growth by inducing growth cone collapse and retraction. The network motif that we have modelled is embedded in a larger, more complex network of molecular interactions that likely contains additional feedback loops. It is possible that such additional feedback loops could be involved in controlling other growth cone behaviours such as collapse and retraction. Previous studies in other systems have shown that incorporating additional feedback loops to a network motif with a positive feedback loop can further contribute towards the regulation of bistable switching behaviour [40,49–52]. For instance, coupling multiple positive feedback loops alters the bistability regime in the parameter space [49,50], interlinking slow and fast positive feedback loops improves the robustness to noise in upstream signalling [51], and negative feedback loops regulate the switching rates between steady states in a network with interlinked positive and negative feedback loops [40]. Our model could thus serve as a starting point to incorporate other molecular interactions and signalling pathways and to identify additional feedback mechanisms involved in axon growth regulation. Extending the model, however, comes at the expense of increased model complexity and additional model parameters, which would need to be tightly constrained by quantitative experimental measurements.

Previous studies have observed stochastic transitions in growth cone cytoskeletal dynamics which could contribute to growth cone state switching behaviour. Betz *et al*. [53,54] identified stochastic switching between bistable on and off states in actin polymerization leading to growth cone membrane protrusion and retraction dynamics. This, however, is unlikely to be the primary cause of growth cone state switching behaviour, as membrane protrusion and retraction cycles are observed in both fast-growing and paused growth cones and occur at a much faster timescale compared to growth switching behaviour [55]. Individual microtubules (MTs) exhibit dynamic instability, i.e. stochastic switching between MT growth and shrinkage phases, which allows MTs to explore the growth cone periphery and regulate growth cone motility. A more detailed model would be required to address how growth cone point contact adhesion and cytoskeleton dynamics act in concert to regulate growth cone switching behaviour.

Growth cone chemotaxis, whereby growth cones sense and grow towards or away from the direction of the molecular gradient in the environment, is another crucial process involved in proper brain wiring [7]. Previous studies have shown that Rac1 regulates growth cone turning responses [56] and molecular gradients asymmetrically regulate PC adhesion dynamics across growth cones [44,57]. These observations suggest that axon growth regulation and growth cone chemotaxis could be interlinked through common signalling pathways. It would be interesting to investigate how changes in growth cone switching behaviour mediated by extracellular signals influence growth cone shape dynamics [41] and axon turning. Previous mathematical models have provided insights into the optimal chemotaxis strategy employed by growth cones to reliably estimate gradient direction [58], the mechanisms involved in gradient amplification [59,60], how intracellular calcium gradients of different steepness are converted into growth cone attraction or repulsion [61,62], and the interactions between the Rho GTPases leading to growth cone turning [63]. A spatially extended framework integrating our model with other models of growth cone chemotaxis would be required to identify mechanistic links between growth cone state switching behaviour and turning responses.

Does stochastic switching between distinct growth cone states play an instructive role in axon pathfinding *in vivo*? A recent study imaging the polarization of guidance receptors in growth cones exposed to molecular gradients found that paused and fast-growing growth cones respond differently to the same extracellular molecular gradient [60]. This suggests that growth cone state changes also affect growth cone chemotactic sensitivity. At the population level, stochastic state switching maintains a fraction of growth cones in the growth state and the rest in the paused state. It is conceivable that growth cone switching behaviour introduces population level diversity in growth cone chemotactic sensitivity. Such diversification of cellular behaviour has been suggested to provide survival advantages for microorganisms in fluctuating environmental conditions [24,64] and performance benefits in bacterial chemotaxis [65,66]. It is thus tempting to speculate a definitive role for growth cone state switching in axonal pathfinding *in vivo*. For instance, the observed growth suppression of all the crossed and uncrossed retinal axons at the optic chiasm during midline crossing [11,67] could be interpreted as a general mechanism to alter switching rates and to regulate population level growth cone chemotactic sensitivity.

Growth cones must generate and exert a force on the environment for axon growth [68–70]. We have modelled how signalling events regulate the PC adhesion dynamics. Our model could be extended to incorporate the mechanical coupling between PCs and the actin network and to provide a direct link between intracellular signalling, traction force generation and axon growth [71,72]. Craig *et al*. [69] modelled conditions where PC adhesions are absent and determined the detailed balance of forces acting on the growth cone actin network required to maintain dynamic actin treadmilling in paused growth cones. Chan & Odde [70] modelled motor-clutch engagement dynamics and suggested substrate stiffness-dependent alterations in these dynamics as a mechanism for the growth cones to sense mechanical signals. Combining these models in the future could provide a better understanding of force generation within the growth cone, and the complex interplay between mechanical and signalling in axon guidance.

Data accessibility. This article has no additional data.

Authors' contributions. P.P. and G.J.G designed the research and wrote the paper. P.P. performed the research.

Competing interests. We declare we have no competing interests.

Funding. This work was supported by the University of Queensland postdoctoral fellowship to P.P., and Australian National Health and Medical Research funding (project grant nos 1083707 and 1107986) to G.J.G.

Acknowledgements. We thank Brendan A. Bicknell for his insightful comments.

References

1. Stoeckli ET. 2012 What does the developing brain tell us about neural diseases? *Eur. J. Neurosci.* **35**, 1811–1817. (doi:10.1111/j.1460-9568.2012.08171.x)
2. Gomez TM, Spitzer NC. 1999 *In vivo* regulation of axon extension and pathfinding by growth-cone calcium transients. *Nature* **397**, 350–355. (doi:10.1038/16927)
3. Mire E *et al.* 2012 Spontaneous activity regulates Robo1 transcription to mediate a switch in thalamocortical axon growth. *Nat. Neurosci.* **15**, 1134–1143. (doi:10.1038/nn.3160)
4. Koser DE *et al.* 2016 Mechanosensing is critical for axon growth in the developing brain. *Nat. Neurosci.* **19**, 1592–1598. (doi:10.1038/nn.4394)
5. Chedotal A, Richards LJ. 2010 Wiring the brain: the biology of neuronal guidance. *Cold. Spring. Harb. Perspect. Biol.* **2**, a001917. (doi:10.1101/cshperspect.a001917)
6. Kolodkin AL, Tessier-Lavigne M. 2011 Mechanisms and molecules of neuronal wiring: a primer. *Cold. Spring. Harb. Perspect. Biol.* **3**, a001727. (doi:10.1101/cshperspect.a001727)
7. Mortimer D, Fothergill T, Pujic Z, Richards LJ, Goodhill GJ. 2008 Growth cone chemotaxis. *Trends Neurosci.* **31**, 90–98. (doi:10.1016/j.tins.2007.11.008)
8. Mason CA, Wang LC. 1997 Growth cone form is behavior-specific and, consequently, position-specific along the retinal axon pathway. *J. Neurosci.* **17**, 1086–1100.
9. Halloran MC, Kalil K. 1994 Dynamic behaviors of growth cones extending in the corpus callosum of living cortical brain slices observed with video microscopy. *J. Neurosci.* **14**, 2161–2177.
10. Mason C, Erskine L. 2000 Growth cone form, behavior, and interactions *in vivo*: retinal axon pathfinding as a model. *J. Neurobiol* **44**, 260–270. (doi:10.1002/1097-4695(200008)44:2<260::AID-NEU14>3.0.CO;2-H)
11. Petros TJ, Rebsam A, Mason CA. 2008 Retinal axon growth at the optic chiasm: to cross or not to cross. *Annu. Rev. Neurosci.* **31**, 295–315. (doi:10.1146/annurev.neuro.31.060407.125609)
12. Argiro V, Bunge MB, Johnson MI. 1984 Correlation between growth form and movement and their dependence on neuronal age. *J. Neurosci.* **4**, 3051–3062.
13. Szebenyi G, Callaway JL, Dent EW, Kalil K. 1998 Interstitial branches develop from active regions of the axon demarcated by the primary growth cone during pausing behaviors. *J. Neurosci.* **18**, 7930–7940.
14. Steketee MB, Oboudiyat C, Daneman R, Trakhtenberg E, Lamoureux P, Weinstein JE, Heidemann S, Barres BA, Goldberg JL. 2014 Regulation of intrinsic axon growth ability at retinal ganglion cell growth cones. *Invest. Ophthalmol. Vis. Sci.* **55**, 4369–4377. (doi:10.1167/iovs.14-13882)
15. Gomez TM, Letourneau PC. 2014 Actin dynamics in growth cone motility and navigation. *J. Neurochem.* **129**, 221–234. (doi:10.1111/jnc.12506)
16. Nichol RI, Hagen KM, Lumbard DC, Dent EW, Gomez TM. 2016 Guidance of axons by local coupling of retrograde flow to point contact adhesions. *J. Neurosci.* **36**, 2267–2282. (doi:10.1523/JNEUROSCI.2645-15.2016)
17. Short CA, Suarez-Zayas EA, Gomez TM. 2016 Cell adhesion and invasion mechanisms that guide developing axons. *Curr. Opin. Neurobiol.* **39**, 77–85. (doi:10.1016/j.conb.2016.04.012)
18. Santiago-Medina M, Gregus KA, Gomez TM. 2013 PAK-PIX interactions regulate adhesion dynamics and membrane protrusion to control neurite outgrowth. *J. Cell Sci.* **126**, 1122–1133. (doi:10.1242/jcs.112607)
19. Woo S, Gomez TM. 2006 Rac1 and RhoA promote neurite outgrowth through formation and stabilization of growth cone point contacts. *J. Neurosci.* **26**, 1418–1428. (doi:10.1523/JNEUROSCI.4209-05.2006)
20. Bokoch GM. 2003 Biology of the p21-activated kinases. *Annu. Rev. Biochem.* **72**, 743–781. (doi:10.1146/annurev.biochem.72.121801.161742)
21. Nayal A, Webb DJ, Brown CM, Schaefer EM, Vicente-Manzanares M, Horwitz AR. 2006 Paxillin phosphorylation at Ser273 localizes a GIT1-PIX-PAK complex and regulates adhesion and protrusion dynamics. *J. Cell Biol.* **173**, 587–589. (doi:10.1083/jcb.200509075)
22. He E, Kapuy O, Oliveira RA, Uhlmann F, Tyson JJ, Novak B. 2011 System-level feedbacks make the anaphase switch irreversible. *Proc. Natl Acad. Sci. USA* **108**, 10 016–10 021. (doi:10.1073/pnas.1102106108)
23. Huang CH, Tang M, Shi C, Iglesias PA, Devreotes PN. 2013 An excitable signal integrator couples to an idling cytoskeletal oscillator to drive cell migration. *Nat. Cell Biol.* **15**, 1307–1316. (doi:10.1038/ncb2859)
24. Acar M, Mettetal JT, van Oudenaarden A. 2008 Stochastic switching as a survival strategy in fluctuating environments. *Nat. Genet.* **40**, 471–475. (doi:10.1038/ng.110)
25. Bhalla US, Iyengar R. 1999 Emergent properties of networks of biological signaling pathways. *Science* **283**, 381–387. (doi:10.1126/science.283.5400.381)
26. Toriyama M, Sakumura Y, Shimada T, Ishii S, Inagaki N. 2010 A diffusion-based neurite length-sensing mechanism involved in neuronal symmetry breaking. *Mol. Syst. Biol.* **6**, 394. (doi:10.1038/msb.2010.51)
27. Cirit M, Krajcovic M, Choi CK, Welf ES, Horwitz AF, Haugh JM. 2010 Stochastic model of integrin-mediated signaling and adhesion dynamics at the leading edges of migrating cells. *PLoS Comput. Biol.* **6**, e1000688. (doi:10.1371/journal.pcbi.1000688)
28. Welf ES, Haugh JM. 2012 Stochastic models of cell protrusion arising from spatiotemporal signaling and adhesion dynamics. *Methods Cell Biol.* **110**, 223–241. (doi:10.1016/B978-0-12-388403-9.00009-6)
29. Holmes WR, Park J, Levchenko A, Edelstein-Keshet L. 2017 A mathematical model coupling polarity signaling to cell adhesion explains diverse cell migration patterns. *PLoS Comput. Biol.* **13**, e1005524. (doi:10.1371/journal.pcbi.1005524)
30. Huang B, Lu M, Jolly MK, Tsarfaty I, Onuchic J, Ben-Jacob E. 2014 The three-way switch operation of Rac1/RhoA GTPase-based circuit controlling amoeboid-hybrid-mesenchymal transition. *Sci. Rep.* **4**, 6449. (doi:10.1038/srep06449)
31. Li X, Saint-Cyr-Proulx E, Aktories K, Lamarche-Vane N. 2002 Rac1 and Cdc42 but not RhoA or Rho kinase activities are required for neurite outgrowth induced by the Netrin-1 receptor DCC (deleted in colorectal cancer) in N1E-115 neuroblastoma cells. *J. Biol. Chem.* **277**, 15 207–15 214. (doi:10.1074/jbc.M109913200)
32. Briancon-Marjollet A *et al.* 2008 Trio mediates netrin-1-induced Rac1 activation in axon outgrowth and guidance. *Mol. Cell. Biol.* **28**, 2314–2323. (doi:10.1128/MCB.00998-07)
33. Toriyama M, Kozawa S, Sakumura Y, Inagaki N. 2013 Conversion of a signal into forces for axon outgrowth through Pak1-mediated shootin1 phosphorylation. *Curr. Biol.* **23**, 529–534. (doi:10.1016/j.cub.2013.02.017)
34. Carlstrom LP, Hines JH, Henle SJ, Henley JR. 2011 Bidirectional remodeling of beta1-integrin adhesions during chemotropic regulation of nerve growth. *BMC Biol.* **9**, 82. (doi:10.1186/1741-7007-9-82)
35. Losick R, Desplan C. 2008 Stochasticity and cell fate. *Science* **320**, 65–68. (doi:10.1126/science.1147888)
36. Qian H. 2012 Cooperativity in cellular biochemical processes: noise-enhanced sensitivity, fluctuating enzyme, bistability with nonlinear feedback, and other mechanisms for sigmoidal responses. *Annu. Rev. Biophys.* **41**, 179–204. (doi:10.1146/annurev-biophys-050511-102240)
37. Das J, Ho M, Zikherman J, Govern C, Yang M, Weiss A, Chakraborty AK, Roose JP. 2009 Digital signaling and hysteresis characterize ras activation in lymphoid cells. *Cell* **136**, 337–351. (doi:10.1016/j.cell.2008.11.051)
38. Bishop LM, Qian H. 2010 Stochastic bistability and bifurcation in a mesoscopic signaling system with autocatalytic kinase. *Biophys. J.* **98**, 1–11. (doi:10.1016/j.bpj.2009.09.055)
39. Warren PB, ten Wolde PR. 2004 Enhancement of the stability of genetic switches by overlapping upstream regulatory domains. *Phys. Rev. Lett.* **92**, 128101. (doi:10.1103/PhysRevLett.92.128101)
40. Avendano MS, Leidy C, Pedraza JM. 2013 Tuning the range and stability of multiple phenotypic states with coupled positive-negative feedback loops. *Nat. Commun.* **4**, 2605. (doi:10.1038/ncomms3605)
41. Goodhill GJ, Faville RA, Sutherland DJ, Bicknell BA, Thompson AW, Pujic Z, Sun B, Kita EM, Scott EK. 2015 The dynamics of growth cone morphology. *BMC Biol.* **13**, 10. (doi:10.1186/s12915-015-0115-7)

42. Tang F, Dent EW, Kalil K. 2003 Spontaneous calcium transients in developing cortical neurons regulate axon outgrowth. *J. Neurosci.* **23**, 927–936.
43. Bechara A *et al.* 2008 FAK-MAPK-dependent adhesion disassembly downstream of L1 contributes to semaphorin3A-induced collapse. *EMBO J.* **27**, 1549–1562. (doi:10.1038/emboj.2008.86)
44. Myers JP, Gomez TM. 2011 Focal adhesion kinase promotes integrin adhesion dynamics necessary for chemotropic turning of nerve growth cones. *J. Neurosci.* **31**, 13 585–13 595. (doi:10.1523/JNEUROSCI.2381-11.2011)
45. Dudanova I, Klein R. 2013 Integration of guidance cues: parallel signaling and crosstalk. *Trends Neurosci.* **36**, 295–304. (doi:10.1016/j.tins.2013.01.007)
46. Zelina P, Avci HX, Thelen K, Pollerberg GE. 2005 The cell adhesion molecule NrCAM is crucial for growth cone behaviour and pathfinding of retinal ganglion cell axons. *Development* **132**, 3609–3618. (doi:10.1242/dev.01934)
47. Skaliora I, Adams R, Blakemore C. 2000 Morphology and growth patterns of developing thalamocortical axons. *J. Neurosci.* **20**, 3650–3662.
48. Godement P, Wang LC, Mason CA. 1994 Retinal axon divergence in the optic chiasm: dynamics of growth cone behavior at the midline. *J. Neurosci.* **14**, 7024–7039.
49. Chang DE, Leung S, Atkinson MR, Reifler A, Forger D, Ninfa AJ. 2010 Building biological memory by linking positive feedback loops. *Proc. Natl Acad. Sci. USA* **107**, 175–180. (doi:10.1073/pnas.0908314107)
50. Tiwari A, Igoshin OA. 2012 Coupling between feedback loops in autoregulatory networks affects bistability range, open-loop gain and switching times. *Phys. Biol.* **9**, 055003. (doi:10.1088/1478-3975/9/5/055003)
51. Brandman O, Ferrell Jr JE, Li R, Meyer T. 2005 Interlinked fast and slow positive feedback loops drive reliable cell decisions. *Science* **310**, 496–498. (doi:10.1126/science.1113834)
52. Padmanabhan P, Garaigorta U, Dixit NM. 2014 Emergent properties of the interferon-signalling network may underlie the success of hepatitis C treatment. *Nat. Commun.* **5**, 3872. (doi:10.1038/ncomms4872)
53. Betz T, Lim D, Kas JA. 2006 Neuronal growth: a bistable stochastic process. *Phys. Rev. Lett.* **96**, 098103. (doi:10.1103/PhysRevLett.96.098103)
54. Betz T, Koch D, Lim D, Kas JA. 2009 Stochastic actin polymerization and steady retrograde flow determine growth cone advancement. *Biophys. J.* **96**, 5130–5138. (doi:10.1016/j.bpj.2009.03.045)
55. Sayyad WA, Amin L, Fabris P, Ercolini E, Torre V. 2015 The role of myosin-II in force generation of DRG filopodia and lamellipodia. *Sci. Rep.* **5**, 7842. (doi:10.1038/srep07842)
56. Yuan XB, Jin M, Xu X, Song YQ, Wu CP, Poo MM, Duan S. 2003 Signalling and crosstalk of Rho GTPases in mediating axon guidance. *Nat. Cell Biol.* **5**, 38–45. (doi:10.1038/ncb895)
57. Hines JH, Abu-Rub M, Henley JR. 2010 Asymmetric endocytosis and remodeling of beta1-integrin adhesions during growth cone chemorepulsion by MAG. *Nat. Neurosci.* **13**, 829–837. (doi:10.1038/nn.2554)
58. Mortimer D *et al.* 2009 Bayesian model predicts the response of axons to molecular gradients. *Proc. Natl Acad. Sci. USA* **106**, 10 296–10 301. (doi:10.1073/pnas.0900715106)
59. Bouzigues C, Holcman D, Dahan M. 2010 A mechanism for the polarity formation of chemoreceptors at the growth cone membrane for gradient amplification during directional sensing. *PLoS ONE* **5**, e9243. (doi:10.1371/journal.pone.0009243)
60. Morel M, Shynkar V, Galas JC, Dupin I, Bouzigues C, Studer V, Dahan M. 2012 Amplification and temporal filtering during gradient sensing by nerve growth cones probed with a microfluidic assay. *Biophys. J.* **103**, 1648–1656. (doi:10.1016/j.bpj.2012.08.040)
61. Forbes EM, Thompson AW, Yuan J, Goodhill GJ. 2012 Calcium and cAMP levels interact to determine attraction versus repulsion in axon guidance. *Neuron* **74**, 490–503. (doi:10.1016/j.neuron.2012.02.035)
62. Sutherland DJ, Pujic Z, Goodhill GJ. 2014 Calcium signaling in axon guidance. *Trends Neurosci.* **37**, 424–432. (doi:10.1016/j.tins.2014.05.008)
63. Sakumura Y, Tsukada Y, Yamamoto N, Ishii S. 2005 A molecular model for axon guidance based on cross talk between rho GTPases. *Biophys. J.* **89**, 812–822. (doi:10.1529/biophysj.104.055624)
64. Kussell E, Leibler S. 2005 Phenotypic diversity, population growth, and information in fluctuating environments. *Science* **309**, 2075–2078. (doi:10.1126/science.1114383)
65. Frankel NW, Pontius W, Dufour YS, Long J, Hernandez-Nunez L, Emonet T. 2014 Adaptability of non-genetic diversity in bacterial chemotaxis. *Elife* **3**, e03526. (doi:10.7554/eLife.03526)
66. Waite AJ, Frankel NW, Dufour YS, Johnston JF, Long J, Emonet T. 2016 Non-genetic diversity modulates population performance. *Mol. Syst. Biol.* **12**, 895. (doi:10.15252/msb.20167044)
67. Wang LC, Rachel RA, Marcus RC, Mason CA. 1996 Chemosuppression of retinal axon growth by the mouse optic chiasm. *Neuron* **17**, 849–862. (doi:10.1016/S0896-6273(00)80217-2)
68. Suter DM, Miller KE. 2011 The emerging role of forces in axonal elongation. *Prog. Neurobiol.* **94**, 91–101. (doi:10.1016/j.pneurobio.2011.04.002)
69. Craig EM, Van Goor D, Forscher P, Mogilner A. 2012 Membrane tension, myosin force, and actin turnover maintain actin treadmill in the nerve growth cone. *Biophys. J.* **102**, 1503–1513. (doi:10.1016/j.bpj.2012.03.003)
70. Chan CE, Odde DJ. 2008 Traction dynamics of filopodia on compliant substrates. *Science* **322**, 1687–1691. (doi:10.1126/science.1163595)
71. Koch D, Rosoff WJ, Jiang J, Geller HM, Urbach JS. 2012 Strength in the periphery: growth cone biomechanics and substrate rigidity response in peripheral and central nervous system neurons. *Biophys. J.* **102**, 452–460. (doi:10.1016/j.bpj.2011.12.025)
72. Hyland C, Mertz AF, Forscher P, Dufresne E. 2014 Dynamic peripheral traction forces balance stable neurite tension in regenerating Aplysia bag cell neurons. *Sci. Rep.* **4**, 4961. (doi:10.1038/srep04961)